Available online at www.sciencedirect.com
ScienceDirect
Computerized Medical Imaging and Graphics 32 (2008) 270–276
Computerized Medical Imaging and Graphics
www.elsevier.com/locate/compmedimag

A comparative study for 2D and 3D computer-aided diagnosis methods for solitary pulmonary nodules

Chinson Yeh [a,1], Jen-Feng Wang [a,2], Ming-Ting Wu [b,c,3], Chen-Wen Yen [a,*], Mark L. Nagurka [d,4], Chen-Liang Lin [a,5]

[a] Department of Mechanical and Electromechanical Engineering, National Sun-Yat Sen University, Kaohsiung, Taiwan ROC
[b] Department of Radiology, Kaohsiung Veterans General Hospital, Kaohsiung, Taiwan ROC
[c] Faculty of Medicine, School of Medicine, National Yang Ming University, Taipei, Taiwan ROC
[d] Department of Mechanical and Biomedical Engineering, Marquette University, Milwaukee, WI, USA

Received 23 April 2007; accepted 14 January 2008

Abstract

Many computer-aided diagnosis (CAD) methods, including 2D and 3D approaches, have been proposed for solitary pulmonary nodules (SPNs). However, the detection and diagnosis of SPNs remain challenging in many clinical circumstances. One goal of this work is to investigate the relative diagnostic accuracy of 2D and 3D methods. An additional goal is to develop a two-stage approach that combines the simplicity of 2D and the accuracy of 3D methods. The experimental results show statistically significant differences between the diagnostic accuracy of 2D and 3D methods. The results also show that with a very minor drop in diagnostic performance the two-stage approach can significantly reduce the number of nodules needed to be processed by the 3D method, streamlining the computational demand.

Keywords: Computer-aided diagnosis; Contrast enhancement; Lung cancer; Solitary pulmonary nodule; Lung nodule; Likelihood of malignancy; Computed tomography

1. Introduction

Lung cancer is the leading cause of cancer death in many regions of the world [1]. Detecting and diagnosing solitary pulmonary nodules (SPNs), the most common manifestation of lung cancer, are critical since early identification of malignant nodules is crucial to the chance for successful treatment [2]. Currently, computed tomography (CT), in particular spiral CT with contrast enhancement, is the imaging modality of choice for SPNs [3]. Previous studies have shown that making an accurate diagnosis based on CT data alone is often a very difficult task [4,5]. As a result, many computer-aided diagnosis (CAD) methods have been proposed for SPNs [6,7]. Based on the dimension of measurements, these CAD methods can be divided into two categories: 2D and 3D methods.

In a 2D CAD method, features that are used to differentiate benign and malignant nodules are generated from a representative (typically the largest) slice of the nodule [4,8–11]. This eliminates the requirement of processing the entire 3D nodule volume and significantly reduces the operational complexity and computational cost that have hindered the application of 3D methods. Another factor that has hampered the development of 3D CAD methods is a limitation of early CT hardware. With single detector row, early CT scanners often generate highly anisotropic image data. For these images, the resolution in the

* Corresponding author at: 70 Lien-hai Road, Kaohsiung 804, Taiwan ROC. Tel.: +886 7 3482965; fax: +886 7 5254299.
E-mail addresses: chinsonyeh@gmail.com (C. Yeh), p923020015@student.nsysu.edu.tw (J.-F. Wang), wu.mingting@gmail.com (M.-T. Wu), vincen@mail.nsysu.edu.tw (C.-W. Yen), mark.nagurka@marquette.edu (M.L. Nagurka), brightkid@gmail.com (C.-L. Lin).
[1] Postal address: 70 Lien-hai Road, Kaohsiung 804, Taiwan ROC. Tel.: +886 7 5254269; fax: +886 7 5254299.
[2] Postal address: 70 Lien-hai Road, Kaohsiung 804, Taiwan ROC. Tel.: +886 7 5254269; fax: +886 7 5254299.
[3] Postal address: 386 Ta-Chung 1st Road, Kaohsiung, 813 Taiwan ROC. Tel.: +886 7 3422121 6205; fax: +886 7 3468301.
[4] Postal address: P.O. Box 1881, Milwaukee, WI 53201-1881, USA. Tel.: +1 414 2883513; fax: +1 414 2887790.
[5] Postal address: 70 Lien-hai Road, Kaohsiung 804, Taiwan ROC. Tel.: +886 7 5254269 6205; fax: +886 7 5254299.

0895-6111/$ – see front matter © 2008 Elsevier Ltd. All rights reserved.
doi:10.1016/j.compmedimag.2008.01.003

axial dimension was typically 10–20 times the size of the in-plane resolution, making accurate 3D nodule modeling very difficult.

With the introduction of multidetector row CT (MDCT), which significantly improves the resolution and acquisition time, scanning the thorax with approximately isotropic 3D resolution without significant breathing artifacts is now possible [12]. Therefore, by employing features that characterize the entire nodule, 3D CAD methods have also been proposed [13–19]. The addition of the extra dimension dramatically increases the operational complexity and computational cost. This is particularly true for nodule segmentation, considered to be one of the most difficult tasks in analyzing SPN images [20–23]. The major challenge for 3D segmentation is that nodules are frequently attached to other structures, such as the local pulmonary vasculature and the pleural surface adjoining the thoracic wall. A fully automatic segmentation method that can separate a nodule from such structures is not available. As a result, laborious, slice-by-slice, manual or semi-automatic segmentation operations are often required.

These additional costs required by the 3D CAD methods maybe worthwhile if the 3D method can provide better diagnostic performance than the 2D method. To the best of our knowledge, this idea has never been studied systematically. Therefore, a first goal of this work is to compare the diagnostic performance of 2D and 3D CAD methods. Considering the operational complexity and the computational cost of the 3D method, a second goal is to develop a criterion to determine which nodules can be diagnosed reliably by the 2D method to minimize the requirement for processing using a 3D method.

2. Methodologies

The computer-aided system used this work is adapted from the work of Yeh et al. [19]. In particular, after using a segmentation method to acquire the 3D nodule volume, features that are used to discriminate the benign and malignant nodules are generated. The procedure is described in Sections 2.2 and 2.3. The following Section 2.1 first introduces the basic methodologies behind these features.

2.1. Perfusion CT and morphometric CT methods

CAD systems for SPNs can be divided into two categories, perfusion CT and morphometric CT methods, based on the nature of features. The diagnostic decisions made by the morphometric CT methods are based on the morphological features, such as shape, size, texture, growth rate and degree of calcification [4,11,13,15,24].

Perfusion CT methods are motivated by the observation that the growth and spread of cancers depend on their ability to induce formation of nearby blood vessels, called angiogenesis [25]. The development of induced new vessels leads to physiological changes, especially increased perfusion, blood volume and capillary permeability [26]. Therefore, the focus of the perfusion CT study is to assess how the CT attenuation value of the nodule changes with time after the injection of a contrast medium. The dynamic behavior can be uncovered by determining attenuation within nodules at several time points after injection of the contrast medium [27]. In comparing the baseline scan with the post-contrast scans, it has been found that benign nodules tend to be enhanced substantially less than the malignant nodules [9,10,28]. Several CAD methods exploit this enhancement property [9,10,16,28–30].

A direct extension of the morphometric CT and perfusion CT based CAD methods is to build a system that employs features of both methods. This design idea has proved to be effective [16,17], and thus the CAD system adopted in this work employs both morphometric and perfusion CT features. The morphometric features used in this study are described in the following subsections.

2.2. Morphometric CT features

One of the drawbacks of some of the previously proposed morphometric CT methods is their dependence on human judgments, such as classifying nodules into one of several predefined shapes [31]. To eliminate the dependence on such subjective decisions, this work uses the 3D moment shape descriptors proposed by Sadjadi and Hall [32] to characterize the morphology of the nodules. This set of 3D moment shape descriptors has several advantages. First, the descriptors can be computed objectively and automatically from the image data. Second, they can be applied to 3D objects without constraints on the object's 3D topology [33]. Third, the 3D moments are invariant to translational shifts, changes of scale and rotations of the image.

To compute 3D moment invariants, the nodule is first represented by the binary image function:

$$O(x, y, z) = \begin{cases} 1 & (x, y, z) \in R \\ 0 & (x, y, z) \notin R \end{cases} \quad (1)$$

where R represents the selected nodule region. For a given set of integers p, q and r, with $n = 1 + (p + q + r) / 3$, the nth order 3D moment μ_{pqr} can be computed from

$$\mu_{pqr} = \sum_{x=1}^{I_X} \sum_{y=1}^{I_Y} \sum_{z=1}^{I_z} O(x, y, z)(x - x_0)^p (y - y_0)^q (z - z_0)^r \quad (2)$$

where (x_0, y_0, z_0) is the centroid of the nodule and I_X, I_Y, I_Z denote the three dimensional image size for the selected nodule region. The corresponding normalized 3D central moments are given by

$$\eta_{pqr} = \frac{\mu_{qpr}}{(\mu_{000})^n} \quad (3)$$

With the normalized 3D central moments, the second order moment invariants derived by Sadjadi are written as

$$M_{21} = \eta_{200} + \eta_{020} + \eta_{002} \quad (4)$$

$$M_{22} = \eta_{200}\eta_{020} + \eta_{200}\eta_{002} + \eta_{020}\eta_{002} - \eta_{110}^2 - \eta_{101}^2 - \eta_{011}^2 \quad (5)$$

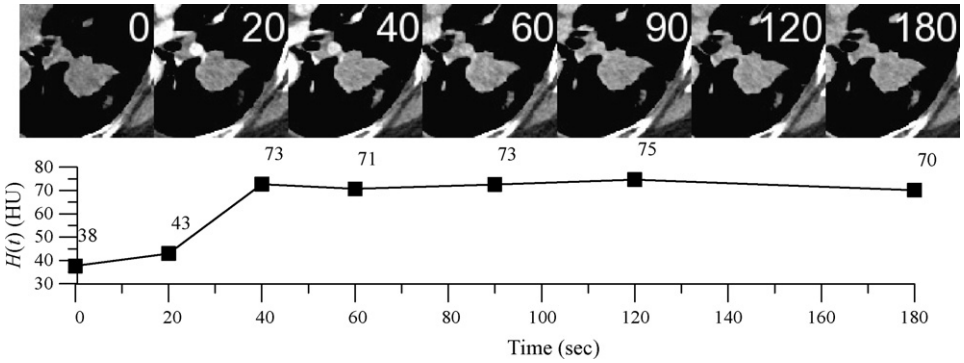

Fig. 1. Serial images with dynamic enhancement curve for a malignant nodule.

$$M_{23} = \eta_{200}\eta_{020}\eta_{002} + 2\eta_{110}\eta_{101}\eta_{011} - \eta_{002}\eta_{110}^2 - \eta_{020}\eta_{101}^2 - \eta_{200}\eta_{011}^2 \quad (6)$$

To expand the set of 3D moment shape descriptors, higher order 3D moment invariants, including third to sixth order moments, have also been developed [34]. However, since higher order moments are more sensitive to noise than lower order moments, this work relies on the three second order 3D moment shape descriptors proposed by Sadjadi and Hall [32].

2.3. Perfusion CT features

In applying the perfusion CT methods, the time period after the injection of the contrast material was divided roughly into two phases [26]: the first pass phase and the delay imagining phase. During the first pass phase, the contrast material is predominantly intravascular. CT scans are typically performed at 20, 40 and 60 s after the injection of the contrast material and used to estimate perfusion and blood volume. During the delay imaging phase, the rate of contrast material passing between vascular and extravascular spaces is bi-directionally balanced. An important property of this phase is that tumors are often characterized by significant return of the contrast material into the intravascular space during the first 2 min after the injection [27]. To identify this property, CT scans are taken at 90, 120 and 180 s after the injection. A sequence of post-contrast nodule images is shown in Fig. 1 to demonstrate this process.

In applying the perfusion CT methods, the time enhancement value TE(t) is defined as

$$\mathrm{TE}(t) = H(t) - H(0) \quad (7)$$

where $H(t)$ is the attenuation value at time t. By taking $t = 0$ as the time of injection, $H(0)$ represents the pre-enhancement attenuation value obtained by the baseline scan.

Typically, the attenuation value $H(t)$ is defined as the average CT value of all the nodule voxels at time t. However, in computing $H(t)$, one modification is employed to improve the flexibility of the perfusion CT method [19]. In computing the TE(t), only the brightest r% of the non-calcified voxels are included. Introducing this inclusion ratio r has several advantages. First, by adjusting the value of r, a series of features can be generated to help classify the nodules. Second, this operation may alleviate the partial volume effect and thus improve the image quality [9,28]. Third, in responding to contrast material, malignant nodules tend to enhance more than the benign nodules. By comparing only the brightest subset of the nodule voxels, the difference may be amplified and nodule classification can become easier. Finally, with the addition of this inclusion ratio r, the perfusion CT features employed in this work are denoted as $\mathrm{TE}_r(t)$.

2.4. Classification methods

To differentiate the nodules, the proposed CAD methods use a neural network ensemble to perform classification [35]. With the multilayered perceptron (MLP) as the base classifier, the neural ensembles are designed by the Bagging method [36]. Several studies have shown that, compared with the standard MLP training method, Bagging can significantly improve the classification accuracy and is also robust to noise [37,38].

To provide reliable estimates for the diagnostic performance of the tested CAD methods, this work divides the dataset into training and testing subsets with a 9:1 ratio. The Bagging method uses the training subset to adjust the connection weights of the MLPs. The testing subset is used to estimate the generalization accuracy of the classifiers. For the sake of reliability, the training process was repeated 2500 times using randomly partitioned training and testing subsets. The means of the classification accuracy, sensitivity, specificity, positive predict value (PPV), negative predict value (NPV), and area under the receiver operating characteristic curve (AUC) are metrics to characterize the diagnostic performance of the tested CAD methods.

In addition to the direct applications of the 2D and 3D methods, this work also introduces a conceptually simple two-stage approach to combine the simplicity of 2D and the accuracy of 3D methods. The 2D and the 3D methods are applied at the first and second stages, respectively. The basic idea of this approach is to try to reliably classify most of the nodules at the first stage using the 2D method. Then only a small portion of nodules requires the second stage processing of the 3D method. The challenge is in determining which nodules are sent to the second stage. This difficulty is resolved by taking advantage of the capability of the MLPs in approximating posterior probabilities [39].

For the nodule classification problem considered in this study, a MLP is trained to approximate the posterior probabilities by

first setting the number of the neural network outputs to two and by specifying the target outputs to be [1,0] and [0,1] for benign and malignant nodules, respectively. After defining the error as the difference between target and actual outputs and using the mean square error as the training error to be minimized, the first and second outputs of the neural network are trained to approximate the posterior probabilities of C_1 (the class of benign nodules) and C_2 (the class of malignant nodules) nodules, respectively. In particular, by denoting $\boldsymbol{x}$ as the neural network input vector and signifying the two neural network outputs as $d_1(\boldsymbol{x})$ and $d_2(\boldsymbol{x})$,

$$d_1(\boldsymbol{x}) \approx P(C_1|\boldsymbol{x}) \tag{8}$$

$$d_2(\boldsymbol{x}) \approx P(C_2|\boldsymbol{x}) \tag{9}$$

According to Bayes' rule for minimum error, the nodule represented by $\boldsymbol{x}$ is assigned to C_1 if

$$P(C_1|\boldsymbol{x}) > P(C_2|\boldsymbol{x}) \tag{10}$$

Otherwise, the nodule is classified into C_2. As the difference between these two posterior probabilities becomes smaller, the classification result will be more sensitive to a neural network training error and thus become less reliable. Based on this property, a nodule is sent to the second stage for further processing only when the MLP outputs used in the first stage satisfy the inequality:

$$d_1(\boldsymbol{x}) - d_2(\boldsymbol{x})| \leq \delta \tag{11}$$

where δ represents a threshold value determined experimentally to balance the efficiency/cost tradeoff of the proposed two-stage approach. Due to the unavailability of the posterior probabilities, in the above inequality, the real posterior probabilities are replaced by the neural network outputs.

The effectiveness of this two-stage approach in improving the computational efficiency of the CAD methods can be characterized by the ratio of the number of nodules that requires only first stage processing to the total number of nodules. Hereafter this ratio is referred to as the efficiency index (EI). A basic design goal of the proposed two-stage method is to maximize the EI while preserving the diagnostic performances of the 3D method as much as possible. Experimental results are reported in the following section to illustrate the design process.

3. Experiments & results

3.1. Materials

From April 2005 to January 2007, a total of 89 patients (58 men and 31 women; age range 30–85 years; mean age 64.5 years ± standard deviation 14.0 years) with SPN based on chest radiography underwent perfusion chest CT. Images were obtained using a 16-detector row CT scanner (Siemens Sensation 16). Scans were performed with 1 mm thickness (0.7 mm interval between two slices and 0.3 mm overlapped), 120 kVp tube voltage, 200–250 mA tube current. Based on the results of a non-enhanced baseline CT scan, the position of the SPN was located by the radiologists and the post-contrast scans were limited to nodule positions to moderate the patient's radiation exposure. Post-contrast scans were performed at 20, 40, 60, 90, 120 and 180 s after intravenous injection of contrast medium (2.0–2.5 ml/s injection rate, 1.0–1.5 ml/kg dose, Optiray 350, Mallinckrodt, Tyco) using a power injector (Missouri, Ulrich, Ulm, Germany).

Of 89 nodules, 58 were malignant (37 men and 21 women; age range 31–85 years; mean age 67.0 ± 13.2 years) and 31 were benign (21 men and 10 women; age range 30–80 years; mean age 59.9 ± 14.4 years). Among the 31 benign nodules, 14 of them were diagnosed as tuberculoma by histological diagnosis or laboratory culture. The remaining 17 were considered benign by histological diagnosis or regressed or were stable during the 2-year follow-up. The sizes (in diameter) of all SPNs were 11.9–110.3 mm (mean diameter 53.2 ± 19.7 mm). There was no significant difference between the diameters of malignant nodules (mean diameter 54.2 ± 18.9 mm; range 13.5–102.6 mm) and benign nodules (mean diameter 51.3 ± 21.3 mm; range 11.9–110.3 mm).

After these scans, image data were reconstructed with a thickness of 1.0 mm. These images were acquired with a 512 × 512 matrix and quantized with 12 bits. With fixed thickness, the actual number of image slices was dependent on the nodule size. The CT data were then transferred to digital imaging and communications in medicine (DICOM) format for analysis.

3.2. Feature selection

In this work, the feature variables for nodule differentiation included three shape moments M_{21}, M_{22} and M_{23} and perfusion CT features $\mathrm{TE}_r(t)$. Ideally, a set of $\mathrm{TE}_r(t)$ should be determined from $0 \leq t < \infty$ and $0 \leq r \leq 100$. However, the values of t were limited to 20, 40, 60, 90, 120 and 180 since the post-contrast CT scans were performed only at these times. To further simplify the problem, for the inclusion ratio r, discrete values of $r = 10$, 20, ..., 100 were considered.

In this work, the tested CAD methods used one morphometric and one perfusion CT feature. The reasons are explained as follows. Conventionally, a perfusion CT based CAD system requires multiple post-contrast scans so that features $\mathrm{TE}_r(t)$ generated from different time points can be used simultaneously. However, by carefully selecting the time for the post-contrast scan, satisfactory diagnostic performance can be achieved with only a single post-contrast scan [19]. This strategy minimizes the amount of radiation exposure to patients and the data processing time. As such, to perform nodule classification, this work used only one perfusion CT feature. Experimental results verify that the diagnostic performance can be improved by combining the perfusion CT feature with the shape moments feature as the shape moments also provide valuable information for nodule classification. To demonstrate this property, Table 1 summarizes the classification accuracy of the shape moment features. Among the tested morphometric CT features, shape moment M_{21} yields the best overall result. The results in Table 1 also show that increasing the number of shape moment features does not improve the diagnostic performance effectively. Hence, the CAD methods tested in this work use only two features: the shape

Table 1
Classification accuracy for the shape moment

Features	Classification accuracy (%) (mean ± standard deviation)
M_{21}	70.8 ± 11.5
M_{22}	69.0 ± 10.5
M_{23}	66.1 ± 9.1
M_{21}, M_{22}	69.9 ± 11.3
M_{21}, M_{22}, M_{23}	68.2 ± 11.0

moment M_{21} and one perfusion feature $TE_r(t)$. For a given time t, the value of r is determined by testing all 10 possible combinations of M_{21} and $TE_r(t)$ for $r = 10, 20, \ldots, 100$. The value of r that yields the best classification accuracy is then selected.

Since finding an optimal set of feature variables is not our goal, the possibility of achieving higher accuracy by using more features has not been investigated comprehensively in this study. However, limited experimental results indicate that the best are likely near optimal.

3.3. Experimental results

In the first part of the experimental results the diagnostic performance metrics of the 2D and 3D methods are compared. The second part studies the effectiveness of the proposed two-stage strategy by comparing its diagnostic performance metrics with those of the 3D methods.

Table 2 summarizes the results of the first part of the experiments and shows the testing subset classification accuracy for both 2D and 3D methods for $t = 20$, 40, 60, 90, 120 and 180. By performing the paired t-test to the results of the 2D and 3D methods obtained from the same scanning time instant, it is found that the p-values are smaller than 10^{-6} for all six cases of post-contrast scanning. These results indicate strongly that the difference between the classification accuracy obtained by the tested 2D and 3D methods are statistically significant. In addition to the classification accuracy, comparative results are given in Table 3 for the two cases that have the highest accuracy ($t = 90$ and $t = 180$). In particular, with the malignancy as the positive class, Table 3 gives the means of sensitivity, specificity, PPV, NPV and AUC for the scanning data for $t = 90$ and $t = 180$.

The second part of the experimental work implements the proposed two-stage approach for $t = 90$. To demonstrate the influence of the threshold value δ used to determine which nodules are sent to the second stage for further processing, the classification accuracy and the percentage of samples that do not require second stage processing are plotted in Fig. 2 as a function of δ. The corresponding sensitivity and specificity are also shown graphically in Fig. 3. Based on the definition of

Table 2
Summary of classification accuracy for 2D and 3D CAD methods

Time of scanning (s)	Inclusion ratio r (%)		Classification accuracy (%) (mean ± standard deviation)	
	CAD methods		CAD methods	
	2D	3D	2D	3D
20	10	10	69.3 ± 13.1	81. 5 ± 11.8
40	100	50	76.9 ± 12.5	87.1 ± 10.2
60	80	80	82.7 ± 11.5	83.5 ± 11.2
90	10	50	81.5 ± 11.6	88.1 ± 10.0
120	50	50	81.2 ± 11.5	86.0 ± 10.5
180	80	40	83.3 ± 11.6	88.9 ± 9.3

Table 3
Summary of diagnostic performance for 2D and 3D CAD methods for $t = 90$ and 180

Diagnostic performance	$t = 90$		$t = 180$	
	CAD methods		CAD methods	
	2D	3D	2D	3D
Sensitivity (%)	90.7	94.4	90.6	96.4
Specificity (%)	61.7	74.4	69.7	73.7
PPV (%)	82.6	88.1	85.7	88.0
NPV (%)	76.9	87.0	78.8	91.2
AUC	0.809	0.858	0.859	0.871

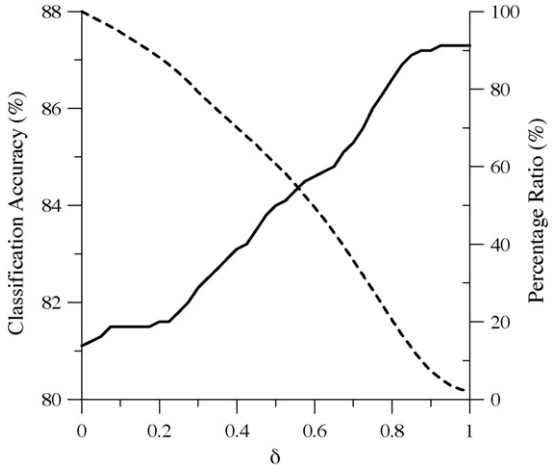

Fig. 2. The cost/accuracy tradeoff of the proposed two-stage strategy for $t = 90$. The solid line is the classification accuracy and the broken line represents the percentage ratio of the nodules that does not require second stage processing.

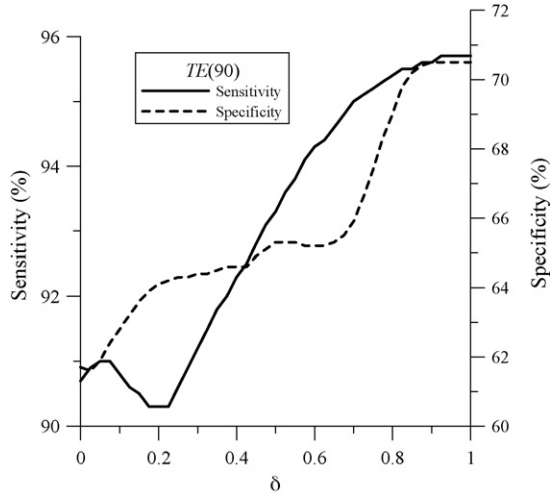

Fig. 3. The corresponding sensitivity and specificity of Fig. 2.

Table 4
Summary of diagnostic performance for 3D method and proposed two-stage strategy for $t = 90$

Diagnostic performances	3D	Two-stage		
Sensitivity (%)	94.4	93.3	92.5	91.5
EI (%)	0	60.7	67.8	76.9
Accuracy (%)	88.1	84.0	83.2	82.5
Specificity (%)	74.4	65.3	64.6	64.4
PPV (%)	88.1	84.3	84.0	83.7
NPV (%)	87.0	83.0	81.2	79.1

δ, it is easy to see that the proposed two-stage strategy transforms into a standard 3D method when δ approaches infinity. Similarly, the proposed two-stage strategy downgrades to a 2D method when δ is set to zero. The results of Fig. 2 demonstrate the accuracy/cost tradeoff of the proposed two-stage strategy. In particular, as δ becomes smaller, fewer nodules require second stage processing and the classification process becomes more efficient. The penalty is increased classification error.

Misclassifying malignant nodules can result in serious consequences in clinical practice. Therefore controlling the percentage of the misclassified malignant nodules by requiring the sensitivity to be sufficiently high is a very important design consideration for the CAD methods. For the proposed two-stage approach, the value of δ can be varied to satisfy such a sensitivity requirement by using the sensitivity versus δ plot of Fig. 3. Table 3 shows that the sensitivity of the 3D method is 94.4 for $t = 90$. By allowing 1%, 2% and 3% drops in sensitivity, Table 4 summarizes the diagnostic performance of the two-stage CAD approaches with sensitivity 93.3%, 92.5% and 91.5%. Compared with the 3D method, the classification accuracy of these three classifiers falls 3.8%, 4.6% and 5.3%, respectively. However, as shown by the values EI, for these three cases, the number of nodules that require 3D method processing is reduced to 39.3%, 32.2% and 23.1%. From these results, by accepting a relatively small diagnostic performance loss, the proposed two-stage approach can improve the computational efficiency significantly.

4. Discussion and conclusion

Despite the common belief that 3D CAD methods can outperform 2D CAD methods in diagnosing solitary pulmonary nodules, to the best of our knowledge, this property has never been investigated systematically. The efficiency/accuracy tradeoff of these methods has also never been studied. By combining morphometric and perfusion CT features, this work performs a comparative study for the 2D and 3D CAD methods for SPNs. As demonstrated by the results of a series of experiments, the diagnostic performance metrics of the 3D method are consistently better than those of the 2D method. Moreover, these differences are also statistically significant.

An important drawback of the 3D method is that it is computationally more intensive and complex than the 2D method. To combine the simplicity of the 2D method and the accuracy of the 3D method, this work proposes a two-stage CAD approach for SPNs. The first stage uses the 2D method to classify nodules. By studying the sensitivity of the decision made by the 2D method to the classifier training error, this work introduces a criterion to estimate the reliability of the classification results made by the 2D method. To improve the computational efficiency and processing complexity, only the nodules that fail to pass this reliability test are sent to the second stage which differentiates nodules by the 3D method. The efficiency/accuracy tradeoff of this two-stage approach can be controlled by adjusting a parameter that characterizes the tolerance of the reliability test. Experimental results show, with a small loss of diagnostic performance, that the efficiency of the computerized diagnosing process can be improved significantly.

This work has restricted the number of features to two. A possible future research direction is to expand the scope using more features. In addition, to more rigorously verify the results obtained in this study, it may be valuable to repeat this work using a more comprehensive dataset.

References

[1] Jemal A, Murray T, Ward E, Samuels A, Tiwari RC, Ghafoor A, et al. Cancer statistics 2005. Cancer J Clin 2005;55:10–30.
[2] Winer-Muram HT. The solitary pulmonary nodule. Radiology 2006;239(1):34–49.
[3] Tan BB, Flaherty KR, Kazerooni EA, Iannettoni MD. The solitary pulmonary nodule. Chest 2003;123(1):89–96.
[4] Shah SK, McNitt-Gray MF, De Zoysa KR, Sayre JW, Kim HJ, Batra P, et al. Solitary pulmonary nodule diagnosis on CT: results of an observer study. Acad Radiol 2005;12(4):496–501.
[5] McCarville MB, Lederman HM, Santana VM, Daw NC, Shochat SJ, Li CS, et al. Distinguishing benign from malignant pulmonary nodules with helical chest CT in children with malignant solid tumors. Radiology 2006;239(2):514–20.
[6] McNitt-Gray M. Lung nodules and beyond: approaches, challenges and opportunities in thoracic CAD. Int Congr Ser 2004;1268:896–901.
[7] Li Q, Li F, Suzuki K, Shiraishi J, Abe H, Engelmann R, et al. Computer-aided diagnosis in thoracic CT. Semin Ultrasound CT MR 2005;25(5):357–63.
[8] McNitt-Gray MF, Wyckoff N, Sayre JW, Goldin JG, Aberle DR. The effects of co-occurrence matrix based texture parameters on the classification of solitary pulmonary nodules imaged on computed tomography. Comput Med Imaging Graph 1999;23(6):339–48.
[9] Yi CA, Lee KS, Kim EA, Han J, Kim H, Kwon OJ, et al. Solitary pulmonary nodules: dynamic enhanced multi-detector row CT study and comparison with vascular endothelial growth factor and microvessel density. Radiology 2004;233(1):191–9.
[10] Jeong YJ, Lee KS, Jeong SY, Chung MJ, Shim SS, Kim H, et al. Solitary pulmonary nodule: characterization with combined wash-in and washout features at dynamic multi-detector row CT. Radiology 2005;237(2):675–83.
[11] Suzuki K, Li F, Sone S, Doi K. Computer-aided diagnostic scheme for distinction between benign and malignant nodules in thoracic low-dose CT by use of massive training artificial neural network. IEEE Trans Med Imag 2005;24(9):1138–50.
[12] Fuchs TOJ, Kachelriess M, Kalender WA, Fast volume scanning approaches by X-ray-computed tomography. In: Proc IEEE Comput Soc Bioinform Conf; 2003;91(10). p. 1492–502.
[13] Kanazawa K, Kawata Y, Niki N, Satoh H, Ohmatsu H, Kakinuma R, et al. Computer-aided diagnosis for pulmonary nodules based on helical CT images. Comput Med Imaging Graph 1998;22(2):157–67.
[14] Kawata Y, Niki N, Ohmatsu H, Moriyama N. Example-based assisting approach for pulmonary nodule classification in three-dimensional thoracic computed tomography images. Acad Radiol 2003;10(12):1402–15.

[15] Awai K, Murao K, Ozawa A, Nakayama Y, Nakaura T, Liu D, et al. Pulmonary nodules: estimation of malignancy at thin-section helical CT-effect of computer-aided diagnosis on performance of radiologists. Radiology 2006;239(1):276–84.
[16] Mori K, Niki N, Kondo T, Kamiyama Y, Kodama T, Kawada Y, et al. Development of a novel computer-aided diagnosis system for automatic discrimination of malignant from benign solitary pulmonary nodules on thin-section dynamic computed tomography. J Comput Assist Tomogr 2005;29(2):215–22.
[17] Shah SK, McNitt-Gray MF, Rogers SR, Goldin JG, Suh RD, Sayre JW, et al. Computer aided characterization of the solitary pulmonary nodule using volumetric and contrast enhancement features. Acad Radiol 2005;12(10):1310–9.
[18] Petkovska I, Shah SK, McNitt-Gray MF, Goldin JG, Brown MS, Kim HJ, et al. Pulmonary nodule characterization: a comparison of conventional with quantitative and visual semi-quantitative analyses using contrast enhancement maps. Eur J Radiol 2006;59(2):244–52.
[19] Yeh C, Lin C-L, Wu M-T, Yen C-W, Wang J-F. A neural network based diagnosis method for characterizing solitary pulmonary nodules. Neurocomputing 2008, doi:10.1016/j.neucom.2007.11.009.
[20] Hu S, Hoffman EA, Reinhardt JM. Automatic lung segmentation for accurate quantitation of volumetric x ray CT images. IEEE Trans Med Imag 2001;20(6):490–8.
[21] Armato SG 3rd, MacMahon H. Automated lung segmentation and computer-aided diagnosis for thoracic CT scans. Int Congr Ser 2003; 1256:977–82.
[22] Kuhnigk JM, Dicken V, Bornemann L, Bakai A, Wormanns D, Krass S, et al. Morphological segmentation and partial volume analysis for volumetry of solid pulmonary lesions in thoracic CT scans. IEEE Trans Med Imag 2006;25(5):417–34.
[23] Reeves AP, Chan AB, Yankelevitz DF, Henschke CI, Kressler B, Kostis WJ. On measuring the change in size of pulmonary nodules. IEEE Trans Med Imag 2006;25(4):435–50.
[24] Reeves AP, Kostis WJ. Computer-aided diagnosis for lung cancer. Radiol Clin North Am 2000;38(3):497–509.
[25] Folkman J, Merler E, Abernathy C, Williams G. Isolation of a tumor factor responsible for angiogenesis. J Exp Med 1971;133(2):275–88.
[26] Miles KA. Tumour angiogenesis and its relation to contrast enhancement on computed tomography: a review. Eur J Radiol 1999;30(3):198–205.
[27] Miles KA. Perfusion CT for the assessment of tumor vascularity: which protocol? Br J Radiol 2003;76(1):36–42.
[28] Swensen SJ, Viggiano RW, Midthun DE, Muller NL, Sherrick A, Yamashita K, et al. Lung nodule enhancement at CT: multicenter study. Radiology 2000;214(1):73–80.
[29] Chang YC, Cheng HH, Yeh CF, Lee WJ, Yang PC, Liu MH, et al. Textural analysis of lung nodule smaller than 3 cm with dynamic contrast enhancement. In: Proc 1st World Congress of Thoracic Imaging and Diagnosis in Chest Disease. 2005.
[30] Gaeta M, Volta S, Bartiromo G, Stroscio S, Minutoli F, Barone M. Contrast-enhanced study of solitary pulmonary nodules with thin-section computed tomography. Radiol Med (Torino) 1997;94(3):189–92.
[31] Li F, Sone S, Abe H, MacMahon H, Doi K. Malignant versus benign nodules at CT screening for lung cancer: comparison of thin-section CT findings. Radiology 2004;233(3):793–8.
[32] Sadjadi FA, Hall EL. Three-dimensional moment invariants. IEEE Trans Pattern Anal Machine Intell 1980;2(2):127–36.
[33] Mangin JF, Poupon F, Duchesnay E, Rivie‘re D, Cachia A, Collins DL, et al. Brain morphometry using 3D moment invariants. Med Imag Anal 2004;8(3):187–96.
[34] Ng B, Abugharbieh R, Huang X, McKeown MJ. Characterizing fMRI activations within regions of interest (ROIs) using 3D moment invariants. In: Proc IEEE 2006 Conf Comput Vision Patt Recog (CVPR). 2006.
[35] Haykin S. Neural network: a comprehensive foundation, 2nd ed. Upper Saddle River, NJ: Prentice Hall; 1999.
[36] Breiman L. Bagging predictors. Mach Learn 1996;24(2):123–40.
[37] Dietterich TG. An experimental comparison of three methods for constructing ensembles of decision trees: bagging, boosting, and randomization. Mach Learn 2000;40(2):139–57.
[38] Opitz D, Maclin R. An empirical evaluation of bagging and boosting for artificial neural networks. In: Conf Rec 1997 IEEE Int Conf Neural Network. 1997.
[39] Bishop CM. Neural Networks for Pattern Recognition. Oxford: Oxford University Press; 1995.

Chinson Yeh received the B.E. and M.E. degrees in mechanical engineering (ME) from National Sun Yat-Sen University, in 1999 and 2001, respectively where he is currently working toward the PhD degree. His research interests include artificial neural network, pattern recognition, and medical imaging analysis, especially the pulmonary nodule detection and diagnosis from chest computer tomography.

Jen-Feng Wang received his B.E. and M.E. degrees in mechanical engineering (ME) and mechanical and electro-mechanical engineering (MEM) from National Sun Yat-Sen University in 2001 and 2003, respectively. He is currently a PhD student at National Sun Yat-Sen University. His research interests include the application of image processing, and neural networks to pattern recognition problems.

Ming-Ting Wu is a section chief of department of radiology at Kaohsiung Veterans General Hospital. He also joined the faculty of medicine, school of medicine at National Yang Ming University. His research works include thoracic & cardiac radiology, functional brain MR spectroscopy and CT coronary angiography.

Chen-Wen Yen received his B.E. degree in mechanical engineering from Tamkang University in 1982 and M.E. and PhD degrees in mechanical engineering from Carnegie-Mellon University in 1986 and 1989, respectively. Following graduation, he joined the faculty in the department of mechanical engineering at Sun Yat-Sen University. The focus of his research work is the application of neural networks on medical imaging applications.

Mark Nagurka earned a PhD in Mechanical Engineering from M.I.T. (Cambridge, MA), taught at Carnegie Mellon University (Pittsburgh, PA), and was a Senior Research Engineer at the Carnegie Mellon Research Institute (Pittsburgh, PA) prior to joining Marquette University (Milwaukee, WI). He is a registered Professional Engineer, a fellow of the American Society of Mechanical Engineers (ASME), and a former Fulbright Scholar. His research interests include mechatronics, automation, control system design, human/machine interaction, and vehicle dynamics.

Chen-Liang Lin received the B.E. and M.E. degrees in mechanical engineering (ME) from National Sun Yat-Sen University, in 1999 and 2001, respectively where he is currently working toward the PhD degree. His research interests include artificial neural network, pattern recognition, and medical signal processing.